Chemically Stable Yttrium and Tin Co-Doped Barium Zirconate Electrolyte for Next Generation High Performance Proton-Conducting Solid Oxide Fuel Cells

*Wenping Sun, Mingfei Liu, and Wei Liu**

$BaZr_{0.7}Sn_{0.1}Y_{0.2}O_{3-\delta}$ (BZSY) is developed as a novel chemically stable proton conductor for solid oxide fuel cells (SOFCs). BZSY possesses the same cubic symmetry of space group *Pm-3m* with $BaZr_{0.8}Y_{0.2}O_{3-\delta}$ (BZY). Thermogravimetric analysis (TGA) and X-ray photoelectron spectra (XPS) results reveal that BZSY exhibits remarkably enhanced hydration ability compared to BZY. Correspondingly, BZSY shows significantly improved electrical conductivity. The chemical stability test shows that BZSY is quite stable under atmospheres containing CO_2 or H_2O. Fully dense BZSY electrolyte films are successfully fabricated on NiO–BZSY anode substrates followed by co-firing at 1400 °C for 5 h and the film exhibits excellent electrical conductivity under fuel cell conditions. The single cell with a 12-μm-thick BZSY electrolyte film outputs by far the best performance for acceptor-doped $BaZrO_3$-based SOFCs. With wet hydrogen (3% H_2O) as the fuel and static air as the oxidant, the peak power density of the cell achieves as high as 360 mWcm^{-2} at 700 °C, an increase of 42% compared to the reported highest performance of $BaZrO_3$-based cells. The encouraging results demonstrate that BZSY is a good candidate as the electrolyte material for next generation high performance proton-conducting SOFCs.

1. Introduction

Solid oxide fuel cells (SOFCs), which can convert chemical energy into electric energy directly at a very high efficiency, is one of the most promising energy conversion systems.[1] Conventional SOFCs is based on yttria/scandia-stabilized zirconia (YSZ/ScSZ) oxide ion conductor and usually operates at temperatures higher than 800 °C. The high operating temperature means high fabrication and operation cost, which is the major cause hindering the commercial application of SOFCs.[2] If the operating temperature can be reduced to intermediate or lower temperatures (below 700 °C), not only can the SOFCs system cost be significantly reduced, but also the maximum theoretical efficiency can be further improved.[3] In order to make stabilized zirconia-based fuel cells more competitive at reduced temperatures, many strategies and fabrication techniques were developed, mainly including optimizing the electrode microstructure of the cells and further decreasing the electrolyte thickness. The peak power density of a ScSZ-based tubular cell was greater than 1 W cm^{-2} at a low temperature of 600 °C after the anode microstructure was well-engineered.[4] Recently, the power density of a YSZ-based cell achieved as high as 1.4 W cm^{-2} at 0.7 V and 600 °C when the electrolyte thickness was decreased to about 1 μm.[5] Fabricating thin-film SOFCs is also a promising approach, and the peak power density of the cell with a 50-nm-thick YSZ electrolyte film and 80-nm-thick Pt electrode layers reached 130 mW cm^{-2} at 350 °C.[6]

Besides, designing highly conductive ionic conductors as electrolytes is another effective strategy to explore high-performance intermediate/low temperature SOFCs. Rare earth-doped ceria (DCO) exhibits very high oxide ionic conductivity, and is considered as a perfect alternative electrolyte material to YSZ.[1,3,7] However, Ce^{4+} in DCO can be easily reduced to Ce^{3+} in fuel atmospheres at elevated temperatures. The reduction behavior would induce serious n-type electronic conduction in DCO, which means partial internal short circuit for a fuel cell. The internal short circuit would result in remarkable decrease of the open circuit voltages (OCVs) and then work efficiency of the cell.[1,3,8] Therefore, to make DCO-based fuel cells really practical, an additional electron-blocking layer must be deposited onto the DCO films to improve the OCVs.[3,9–13] After depositing a 3-μm-thick YSZ thin film, the OCV of the $Ce_{0.9}Gd_{0.1}O_{1.95}$-based cell was significantly improved, increasing

W. P. Sun, Prof. W. Liu
CAS Key Laboratory of Materials for Energy Conversion
Department of Materials Science and Engineering
University of Science and Technology of China (USTC)
Hefei 230026, P.R. China
E-mail: wliu@ustc.edu.cn
Prof. W. Liu
Key Laboratory of Materials Physics
Institute of Solid State Physics
Chinese Academy of Sciences
Hefei 230031, P.R. China
Dr. M. F. Liu
Center for Innovative Fuel Cell and Battery Technologies
School of Materials Science and Engineering
Georgia Institute of Technology
Atlanta, GA 30332, USA

DOI: 10.1002/aenm.201201062

from 0.59 to 1.05 V at 800 °C.[9] The OCV of a $Ce_{0.8}Sm_{0.2}O_{2-\delta}$-based cell increased to 1.04 V at 700 °C by incorporating a thin BaO-CeO_2-Sm_2O_3 composite electron-blocking interlayer in situ at the anode/electrolyte interface.[13] High-temperature proton conductors (HTPCs) are also promising electrolytes for intermediate/low temperature SOFCs, where the corresponding cell is generally named as proton-conducting SOFCs. In the past decade, HTPCs, especially acceptor-doped $BaCeO_3$ and $BaZrO_3$ perovskite oxides, attracted much attention and were investigated extensively. Compared with the typical oxide ion conductors, e.g. YSZ and DCO, proton transport in HTPCs is much easier and the apparent activation energy is much lower than that for oxide ion transport. Lower activation energy helps HTPCs to exhibit superior conductivity at reduced temperatures, and the conductivity is still higher than 0.01 S cm^{-1} at 600 °C.[14–16] Notably, compared to DCO, the electronic conductivity of acceptor-doped $BaCeO_3$ and $BaZrO_3$ under fuel cell conditions is much lower, which is highly desired for fuel cells. The sufficiently high low-temperature conductivity facilitates proton-conducting SOFC to output high power densities at reduced operating temperatures. As the most popular HTPCs, both acceptor-doped $BaCeO_3$ and $BaZrO_3$ perovskites have their own drawbacks. Acceptor-doped $BaCeO_3$ exhibits very poor chemical stability against H_2O and CO_2.[17,18] Considering the terrible chemical stability, acceptor-doped $BaCeO_3$ is difficult to meet the demand of practical applications, where long-term operation is required. In contrast, acceptor-doped $BaZrO_3$ are quite chemically stable;[18–22] however, they are highly refractory with low rates of grain growth and thus have high grain boundary density, which is extremely detrimental to the total electrical conductivity.[16,19] As a result, fabrication of highly conductive $BaZrO_3$-based films via traditional ceramic processes is still a great challenge to date. Generally, preparing ultrathin $BaZrO_3$-based electrolyte films is an effective approach to decrease the contribution of ohimc resistance to the fuel cell. A peak power density of 110 mW cm^{-2} at 600 °C was achieved for an anode-supported cell with a 4-μm-thick $BaZr_{0.8}Y_{0.2}O_{3-\delta}$ (BZY) electrolyte film fabricated by pulsed laser deposition (PLD).[23] Shim et al.[24] reported a thin-film SOFC with BZY electrolyte, and the peak power density of the cell with a 110-nm-thick BZY film prepared by atomic layer deposition (ALD) was as high as 136 mW cm^{-2} at 400 °C. However, it must be mentioned that both PLD and ALD techniques are only suitable for small-scale applications and will introduce additional fabrication cost. Further, although the properties of $BaCeO_3$-$BaZrO_3$ solid solution have been proved to compromise between those single oxides,[14,15,25] the chemical stability is still the bottleneck. It has been reported that the solid solution would react with CO_2 as long as cerium appears in the B site of the perovskite.[18,26] Therefore, exploring chemically stable and highly conductive HTPCs and fabricating corresponding high-quality dense films is becoming increasingly urgent to promote the development of proton-conducting SOFCs.

In this work, yttrium and tin co-doped barium zirconate was developed as a new proton conductor with high chemical stability and sufficient electrical conductivity. $BaZr_{0.7}Sn_{0.1}Y_{0.2}O_{3-\delta}$ (BZSY) was synthesized and evaluated as an electrolyte material for proton-conducting SOFCs. The chemical stability and electrical conductivity were investigated. Dense and highly conductive BZSY electrolyte films supported by porous anodes were successfully fabricated. And the electrochemical performance of the BZSY-based single cell was also evaluated.

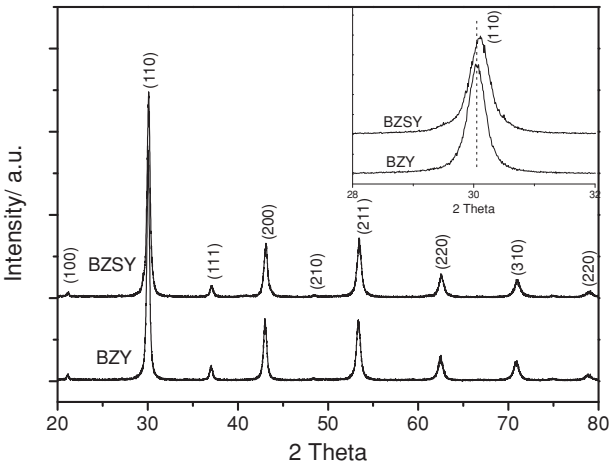

Figure 1. XRD patterns of the BZSY and BZY powders prepared by the combustion method after calcined at 1100 °C for 6 h. Inset: magnified XRD patterns for $28° \leq 2\theta \leq 32°$.

2. Results and Discussion

2.1. Powder Characterization

Figure 1 shows the XRD patterns of the BZSY and BZY powders prepared via the combustion method after calcined at 1100 °C for 6 h in air. Indexing of these patterns clearly reveals that BZSY possesses the same cubic symmetry of space group *Pm-3m* with BZY. The characteristic peaks of BZSY shift toward higher reflection angles compared to BZY. The lattice parameters (*a*) were calculated to be 4.1979(8) Å and 4.2048(3) Å for BZSY and BZY, respectively. The ionic radii of six coordinated Sn^{4+} and Zr^{4+} are 0.69 Å and 0.72 Å, respectively.[27] Thus, the decrease in lattice parameter after Sn substitution reflects the substantial substitution of Sn^{4+} for Zr^{4+} in the lattice.

The surface chemical states of the BZSY and BZY powders were analyzed by XPS, as shown in **Figure 2**. All peak positions are corrected by the C 1s peak at 284.77 eV, which is due to contamination on the powders. Core levels of Ba $3d_{5/2}$, Ba $3d_{3/2}$, Zr 3d, Y 3d, Sn $3d_{5/2}$, Sn $3d_{3/2}$, and O 1s can be identified in the survey spectroscopy (Figure 2(a)). The fine spectra of Ba $3d_{5/2}$, Ba $4p_3$, Zr $3d_{5/2}$, Zr $3d_{3/2}$, Y $3d_{5/2}$, Y $3d_{3/2}$, O 1s, Sn $3d_{5/2}$, and Sn $3d_{3/2}$ peaks for BZY and BZSY are presented in Figure 2(b)-(f). As can be seen, the binding energy (BE) values of Ba $3d_{5/2}$, Ba $3d3_{/2}$, and Ba $4p_3$ core levels don't change at all after incorporating Sn into BZY lattice. Compared to those for BZY, the Zr $3d_{5/2}$, Zr $3d_{3/2}$, Y $3d_{5/2}$, Y $3d_{3/2}$, and O 1s peaks for BZSY all exhibit chemical shifts to the lower binding energy region. The chemical shifts might be attributed to the fine Zr–O and Y–O bonds change of coordination environment in $BaZrO_3$.[28] Due to the difference in the cation sizes of Zr^{4+} and Sn^{4+}, the perfect ZrO_6 octahedra should be distorted, and correspondingly results in the change of BE values and lattice

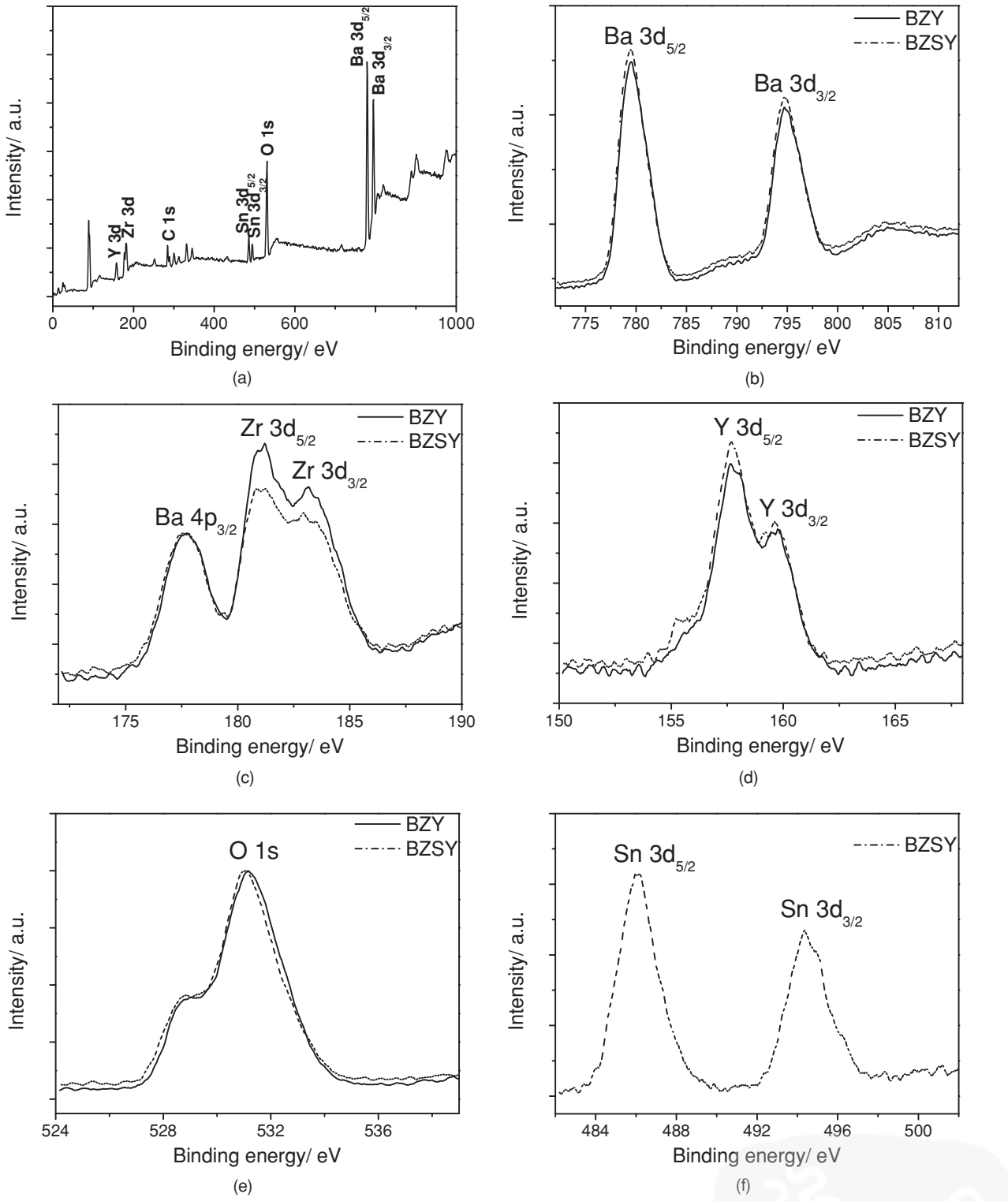

Figure 2. XPS spectra of BZSY and BZY powders: (a) survey, (b) Ba 3d, (c) Zr 3d and Ba 4p, (d) Y 3d, (e) O 1s, (f) Sn 3d.

parameters. The change of lattice parameters is already verified by the XRD result. The BE value of O 1s is a good basicity scale for oxides and decreases with increasing basicity.[29–32] Notably, a high basicity of the oxide favors the formation of the proton defects.[33,34] Thus, proton defects are expected to form more easily in BZSY. Moreover, we also find that, in hydrated samples, O 1s peaks for BZSY shifts to the lower binding energy region as well. It has been reported that O1s peak at lower

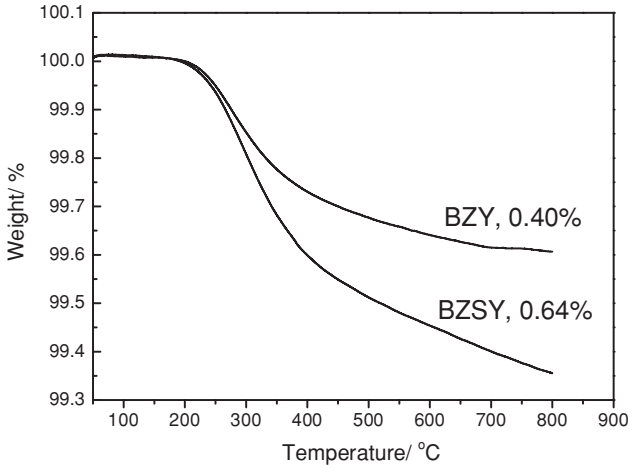

Figure 3. TGA curves of hydrated BZSY and BZY powders with a heating rate of 5 °C min^{-1} in flowing air.

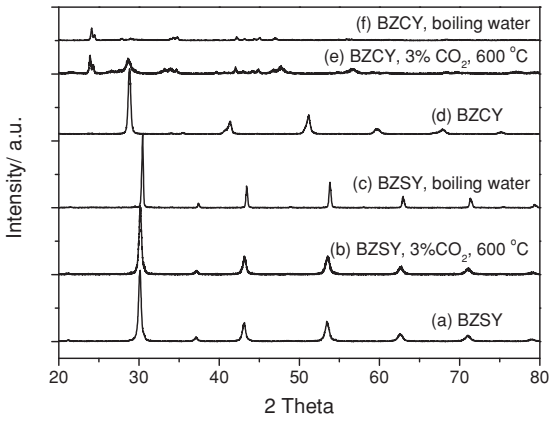

Figure 4. XRD patterns: BZSY powders before (a) and after exposure to wet 3% CO_2 at 600 °C for 10 h (b), (c) BZSY pellet after exposure to boiling water for 4 h, BZCY powders before (d) and after exposure to wet 3% CO_2 at 600 °C for 10 h (e), (f) BZCY pellet after exposure to boiling water for 4 h.

binding energy side corresponds to a higher surface OH density.[35,36] Therefore, we can deduce that the proton concentration of BZSY would be higher than that of BZY after hydration. The Sn $3d_{5/2}$ and Sn $3d_{3/2}$ spectra obtained from BZSY powders correspond to two distinguishable peaks with BE values of about 486.1 and 494.5 eV, respectively, and the BE splitting is about 8.4 eV. According to the present results, the main oxidation state of Sn should be Sn^{4+} in BZSY.[37,38] Besides, the intensities of Zr $3d_{5/2}$ and Zr $3d_{3/2}$ peaks decrease correspondingly compared to those for BZY, further confirming the substantial substitution of Sn^{4+} for Zr^{4+} in BZSY.

TGA was carried out on hydrated BZSY and BZY powders to evaluate the hydration behavior, as shown in **Figure 3**. Weight loss can be observed for the two samples, and reaches 0.64% and 0.40% when heated to 800 °C for BZSY and BZY, respectively. The weight loss of BZSY is slightly more compared to BZY, indicating that BZSY is hydrated more severely. The hydration behavior of the oxide powders under wet atmospheres is mainly contributed by the dissociative adsorption reaction of water. Usually, water dissociates into a hydroxide ion and a proton firstly; then, the hydroxide ion fills an oxygen vacancy in the oxide, and the proton forms a covalent bond with the lattice oxygen.[39] The Kroger–Vink notation for this reaction can be described by Eq. (1),

$$H_2O(g) + O_O^{\times} + V_O^{\bullet\bullet} \rightarrow 2OH_O^{\bullet} \quad (1)$$

In other words, we can conclude that BZSY is capable of incorporating more protons into the crystal lattice after partial substitution of Sn^{4+} for Zr^{4+}. Interestingly, the TGA result is in accordance with the XPS result as discussed above. The increased proton concentration is beneficial for enhancing proton conductivity.

2.2. Chemical Stability

In practical applications, proton conductors must exhibit excellent chemical resistance to a variety of acidic gases (mainly CO_2) and water vapor. For proton-conducting SOFCs, water vapor not only exists at the anode/electrolyte interface but also is formed at the cathode/electrolyte interface during operation. At the same time, the cathode/electrolyte interface has to face CO_2 coming from air. If the electrolyte cannot tolerate the corrosion from water vapor or CO_2, the electrode/electrolyte interface and even the whole cell would break down gradually. To evaluate the chemical stability against CO_2 and water vapor, BZSY powders and sintered pellets were treated in atmospheres containing water vapor or CO_2 and boiling water. The XRD patterns of the fresh and treated BZSY samples are shown in **Figure 4**. As can be seen, the structure of BZSY powders remains unchanged after exposed to a wet atmosphere containing 3% CO_2 at 600 °C for 10 h, and no other phases can be found when the BZSY pellet was treated in boiling water for 4 h. While for $BaZr_{0.1}Ce_{0.7}Y_{0.2}O_{3-\delta}$ (BZCY), which was also reported as a stable proton conductor, not only the powders but also the pellet was totally decomposed after exposed in the same atmospheres as BZSY. The chemical stability test reveals that BZSY shows excellent H_2O and CO_2 tolerance and is a promising chemically stable proton conductor for practical applications.

2.3. Conductivity

Electrochemical impedance spectra were performed to investigate the electrical conduction behavior of BZSY in different atmospheres. In addition, the conductivity of the state-of-the-art stable proton conductor BZY was also studied comparatively. Shown in **Figure 5** is a typical SEM image of the cross-sectional morphology of the sintered BZSY pellet used for conductivity measurement. The BZSY pellet is still very porous after high-temperature sintering and the grain size is less than 1 μm. The relative density of the pellets is only about 83% and 80% for BZSY and BZY, respectively. This result suggests that the sintering activity of BZSY is sill as poor as most of the acceptor-doped $BaZrO_3$ materials, and much work remains to be done to promote the sintering of BZSY. **Figure 6**(a) presents the temperature dependence of the total conductivity of BZSY and

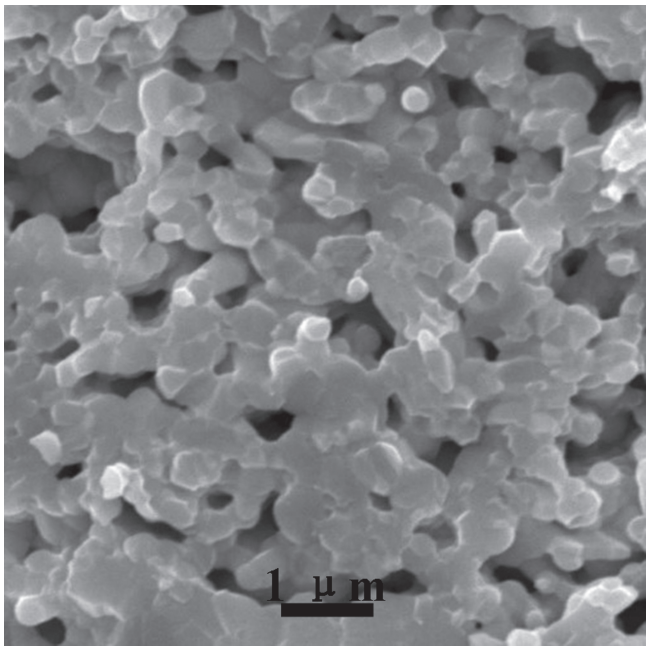

Figure 5. The SEM image of the cross-sectional morphology of the sintered BZSY pellet.

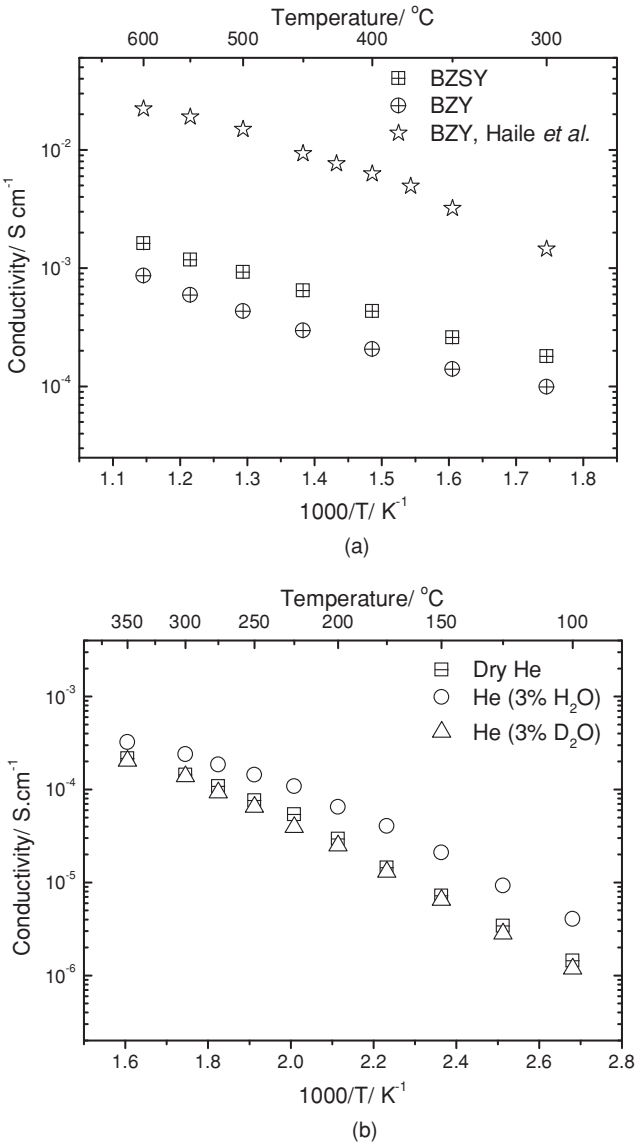

Figure 6. (a) Arrhenius plots of the total electrical conductivity of BZSY and BZY pellets in wet hydrogen (3% H_2O). (**b**) Arrhenius plots of the total electrical conductivity of BZSY pellet in dry and wet He.

BZY in wet H_2 (3% H_2O), and the total conductivity of BZY in wet N_2 reported by Haile et al.[16] is inserted for comparison. Clearly, the conductivity of BZSY is higher than that of BZY, indicating that proton conduction is enhanced after incorporating Sn into BZY lattice. The total electrical conductivity of BZY in wet H_2 is 8.6×10^{-4} S cm^{-1} at 600 °C, while the conductivity increases to 1.6×10^{-3} S cm^{-1} for BZSY. At the same time, the apparent activation energy E_a is calculated to be 0.37 and 0.38 eV for BZY and BZSY, respectively. As discussed above, BZSY is able to absorb more water vapor compared to BZY, which means more protons can be inserted into the BZSY crystal lattice. The improved electrical conductivity of BZSY is very probably induced by the higher proton concentration. Additionally, the slightly higher relative density of BZSY is also beneficial for obtaining higher conductivity. However, it should be mentioned that the electrical conductivity of BZY and BZSY in the present work is lower than the results reported by Haile et al. (Figure 6(a)) and some other groups.[16,20,21] As reported, the conductivity of $BaZrO_3$-based materials is significantly dependent on the fabrication process of the samples and usually span over several orders of magnitude.[40] The low conductivity in this work might be mainly caused by the low relative density of the pellets as well as the small grain size, which would induce high grain boundary resistance.[16,21] Besides, the chemical composition variation, especially Ba evaporation during high-temperature sintering, might also play an important role in this case.[40,41] Whatever, the conductivity improvement is substantial after Sn incorporation. It can be anticipated that the conductivity of BZSY will be certainly further increased by means of optimizing the preparation procedure of the samples. H_2O/D_2O exchange measurement was also performed at low temperatures to verify that protons are the main charge carriers in BZSY in wet atmospheres. A notable difference in the conductivity of BZSY measured in wet (3% H_2O) and dry He can be observed (Figure 6(b)). The conductivity in wet He (3% H_2O) is much higher than that in dry He. The conductivity enhancement should be correlated with the response of proton conduction in wet atmosphere. The apparent activation energy E_a for the conductivity in dry He is calculated to be 0.46 eV, while the E_a value decreases to 0.40 eV in wet He (3% H_2O). Further, as can be seen from Figure 6(b), the conductivity doesn't recover when the atmosphere is switched from dry He to He (3% D_2O). The conductivity ratio $\sigma(H_2O)/\sigma(D_2O)$ varies between 1.6 and 3.4, but deviates from the ideal value of 1.414.[42] Similar phenomenon was also observed in some other proton-conducting oxides at low temperatures.[21,22,42] Even so, the isotope effect can still verify the proton conduction behavior of BZSY.

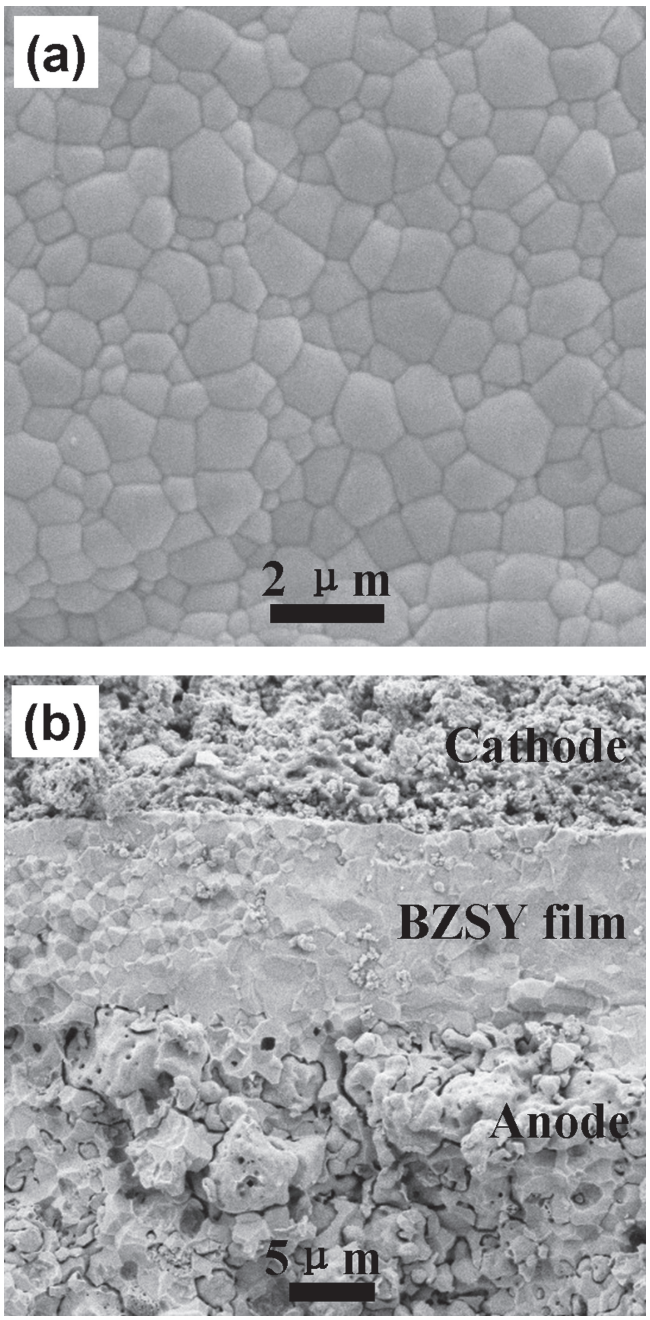

Figure 7. SEM images of the surface morphology of the as-sintered BZSY electrolyte film (a) and the cross section of the tested single cell (b).

2.4. SOFC Applications

In order to further evaluate the potential of BZSY as an electrolyte for SOFCs, dense BZSY films were successfully deposited on porous anodes by a drop-coating process followed by co-firing at 1400 °C for 5 h. Single cells were assembled with $Sm_{0.5}Sr_{0.5}CoO_{3-\delta}$–$Ce_{0.8}Sm_{0.2}O_{2-\delta}$ (SSC–SDC) as cathode. Wet hydrogen (3% H_2O) and static air was used as the fuel and the oxidant, respectively. **Figure 7** shows the SEM images of the surface morphology of the as-sintered BZSY electrolyte film and the cross section of the tested cell. As can be seen from the surface morphology (Figure 7(a)), the BZSY film is totally dense and the grain size ranges from hundreds of nanometers to around 2 μm. From the cross-sectional view of the cell (Figure 7(b)), we can also find that the BZSY film is about 12 μm in thickness, fully dense, and free of any pores. Apart from blocking gas leakage during operation, the high-quality BZSY film definitely ensures fast proton transport through the electrolyte and thereby decrease internal resistance of the single cell. In addition, it seems that the electrode/electrolyte interfaces of the cell are pretty good, where the electrode layers adhere firmly to the electrolyte film. Notably, the well-established configuration is quite in favor of mass and charge transfer in the cell and thus attaining good electrochemical performance. Shown in **Figure 8**(a) are the *I–V* and power density curves of the single cell measured at different operating temperatures. The OCVs

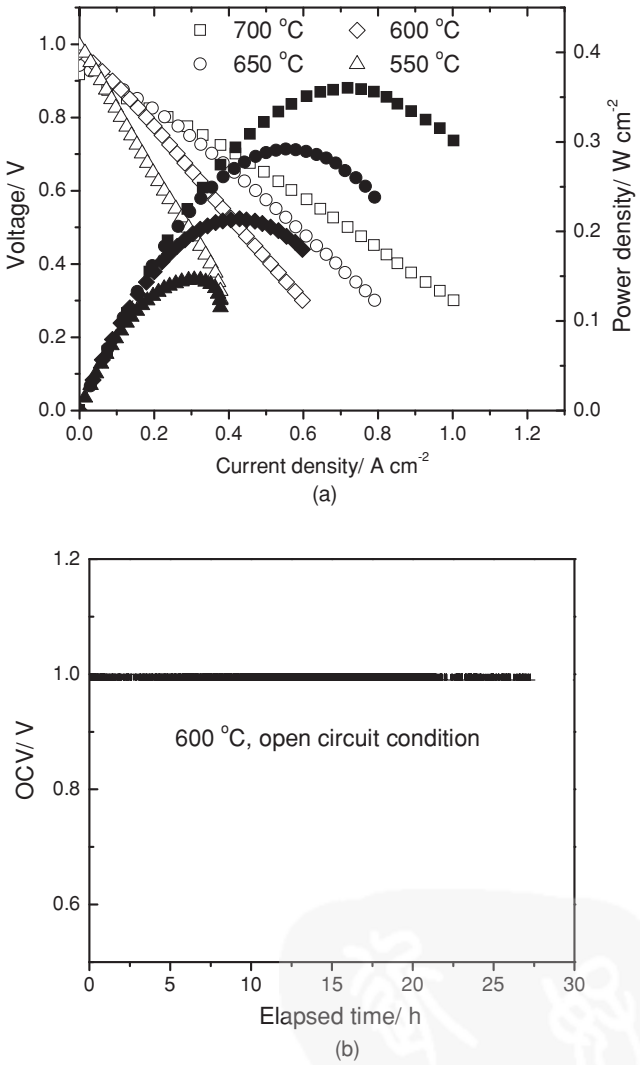

Figure 8. (a) *I–V* and power density curves of the single cell at different operating temperatures with wet hydrogen (3% H_2O) as the fuel and static air as the oxidant. (b) Short-term stability of OCV of the single cell at 600 °C.

Table 1. Summary of the peak power density (mW cm^{-2}), electrolyte film thickness (μm) and conductivity (S cm^{-1}), ohmic (R_{ohm}, Ω cm^2) and polarization resistance (R_p, Ω cm^2), and open circuit voltage (OCV, V) of anode supported proton-conducting SOFCs with acceptor-doped $BaZrO_3$ electrolytes reported in literatures.

Electrolyte	Film fabrication method	Film thickness	Electrode materials (Anode; Cathode)	Peak power density	R_{ohm}	R_p	Film conductivity	OCV	Ref.
$BaZr_{0.8}Y_{0.2}O_{3-\delta}$	Dry pressing	30	Ni-BZY; BSCF	45 (700 °C)	-	-	-	0.94	[26]
$BaZr_{0.8}Y_{0.2}O_{3-\delta}$	Dry pressing	20	Ni-BZCY; SSC-SDC	170 (700 °C)	0.67	0.28	2.99×10^{-3}	0.953	[51]
$BaZr_{0.8}Y_{0.2}O_{3-\delta}$	PLD	4	Ni-BZY; LSCF-BCYb	110 (600 °C)	1.85	0.56	2.16×10^{-4}	0.99	[23]
$BaZr_{0.9}Y_{0.1}O_{3-\delta}$	Dry pressing	20	Ni-BZY; PBC-BZPY	254 (700 °C)	0.53	0.073	3.77×10^{-3}	0.9	[43]
$BaZr_{0.8}Y_{0.2}O_{3-\delta}$-Li	Dry pressing	25	Ni-BZY; LSCF-BZY	53 (700 °C)	0.95	1.66	2.63×10^{-3}	0.98	[52]
$BaZr_{0.8}Y_{0.2}O_{3-\delta}$-CaO	Dry pressing	25	Ni-BZY; LSCF-BZY	141 (700 °C)	1.19	0.25	2.1×10^{-3}	0.99	[53]
$BaZr_{0.8}Y_{0.2}O_{3-\delta}$	Dry pressing	30	Ni-BZY; LSCF-BZPY	172 (700 °C)	0.56	0.25	5.4×10^{-3}	0.9	[54]
$BaZr_{0.7}Pr_{0.1}Y_{0.2}O_{3-\delta}$	Dry pressing	20	Ni-BZY; LSCF-BZPY	81 (600 °C)	1.33	1.3	1.5×10^{-3}	0.93	[21]
$BaZr_{0.8}In_{0.2}O_{3-\delta}$	Dry pressing	20	Ni-BZCY; SSC-SDC	85 (700 °C)	1.84	0.68	1.1×10^{-3}	0.95	[22]
$BaZr_{0.7}Pr_{0.1}Y_{0.2}O_{3-\delta}$	Dry pressing	12	Ni-BZY; LSCF-BZPY30	163 (600 °C)	0.53	0.53	2.26×10^{-3}	0.97	[55]
$BaZr_{0.7}In_{0.3}O_{3-\delta}$	Dry pressing	15	Ni-BZI; PBC-BZPY	84 (600 °C)	2.01	0.27	7.46×10^{-4}	0.946	[56]
$BaZr_{0.8}Y_{0.2}O_{3-\delta}$	Drop coating	25	Ni-BZCY; SSC-SDC	55 (600 °C)	3.24	1.98	7.72×10^{-4}	0.97	[57]
$BaZr_{0.8}Y_{0.16}Zn_{0.04}O_{3-\delta}$	Spin coating	20	Ni-BZY; Pt	75 (600 °C)	1.15	2.6	1.74×10^{-3}	0.94	[58]
$BaZr_{0.7}Sn_{0.1}Y_{0.2}O_{3-\delta}$	Drop coating	12	Ni-BZSY; SSC-SDC	360 (700 °C)	0.20	0.13	6.0×10^{-3}	0.92	This work
				214 (600 °C)	0.46	0.41	2.6×10^{-3}	0.98	

$Ba_{0.5}Sr_{0.5}Co_{0.8}Fe_{0.2}O_{3-\delta}$ (BSCF), $Sm_{0.5}Sr_{0.5}CoO_{3-\delta}$ (SDC), $Ce_{0.8}Sm_{0.2}O_{2-\delta}$ (SDC), $La_{0.6}Sr_{0.4}Co_{0.2}Fe_{0.8}O_{3-\delta}$ (LSCF), $BaCe_{0.9}Yb_{0.1}O_{3-\delta}$ (BCYb), $BaZr_{0.8}Y_{0.2}O_{3-\delta}$ (BZY), $PrBaCo_2O_{5+\delta}$ (PBC), $BaZr_{0.7}Pr_{0.1}Y_{0.2}O_{3-\delta}$ (BZPY), $BaZr_{0.1}Ce_{0.7}Y_{0.2}O_{3-\delta}$ (BZCY), $BaZr_{0.5}Pr_{0.3}Y_{0.2}O_{3-\delta}$ (BZPY30), $BaZr_{0.7}In_{0.3}O_{3-\delta}$ (BZI).

of the cell reached 0.92, 0.96, 0.98, and 1.0 V at 700, 650, 600, and 550 °C, respectively. And the values are comparable with other $BaZrO_3$-based single cells (**Table 1**). The high OCV values confirm that the BZSY electrolyte is dense enough to prevent gas leakage, which is consistent with the SEM results (Figure 7). The peak power densities of the cell achieved 360, 292, 214, and 146 mW cm^{-2} at 700, 650, 600, and 550 °C, respectively. It must be mentioned that the power performance is by far the best among those ever-reported proton-conducting SOFCs with $BaZrO_3$-based electrolytes, as summarized in Table 1. The peak power density at 700 °C improves as high as 42% compared to the reported highest performance of $BaZrO_3$-based cells in literatures, the value of which was 254 mW cm^{-2}.[43] And the cell performance is comparable with and even better than many $BaCeO_3$-based proton-conducting SOFCs.[14,44–50] The result is definitely a significant progress for the proton-conducting SOFCs field, which demonstrates that desirable electrochemical performance can be obtained using $BaZrO_3$-based electrolytes and BZSY is indeed a promising electrolyte material for low-temperature proton-conducting SOFCs. The chemical stability of BZSY under fuel cell conditions was also evaluated, as shown in Figure 8(b). The OCV of the cell still kept constant after operating for 27 h under open circuit conditions, suggesting that no degradation and no gas leakage occurred during operation. The short-term stability testing confirms that BZSY is a chemically stable proton conductor.

Electrochemical impedance spectra of the cell were measured under open circuit conditions to further investigate the dependence of the cell resistances on the operating temperature, as shown in **Figure 9**(a). In the spectra, the intercept with the real axis at high frequencies represents the ohmic resistance (R_{ohm}) of the cell, which is mainly contributed by the electrolyte resistance, and the difference between the high frequency and the low frequency intercept with the real axis represents the polarization resistance (R_p) of the cell. As can be seen, both R_{ohm} and R_p increase significantly with decreasing the operating temperature. Figure 9(b) shows R_{ohm}, R_p and the total resistances ($R_t = R_{ohm}+R_p$) of the cell estimated from the impedance spectra. R_{ohm} is 0.2, 0.34, 0.46, and 0.71 Ω cm^2, and R_p is 0.13, 0.19, 0.41, and 1.32 Ω cm^2 at 700, 650, 600, and 550 °C, respectively. Clearly, at temperatures higher than 600 °C, R_{ohm} dominates the total resistance, indicating it should be more important to decrease R_{ohm} to further improve the cell performance. Yet, at low temperatures, more attention should be paid to decrease R_p. As R_{ohm} is dominated by the electrolyte resistance, we can estimate the conductivity of the BZSY electrolyte film under fuel cell conditions based on the R_{ohm} values and film thickness, and the result is shown in Figure 9(c). The estimated conductivity of BZSY film achieves about 6.0×10^{-3}, 3.5×10^{-3}, 2.6×10^{-3}, and 1.7×10^{-3} S cm^{-1} at 700, 650, 600, and 550 °C, respectively. Notably, this film shows the highest conductivity among $BaZrO_3$-based films fabricated via the traditional ceramic process, such as dry pressing and coating, as shown in Table 1, and this should be one of the most essential reasons to interpret the high performance of the cell. The conductivity of BZY film prepared by a dry-pressing technique was calculated to be only about 2.99×10^{-3}, 2.15×10^{-3}, 1.43×10^{-3}, 1.0×10^{-3} S cm^{-1} at 700, 650, 600, and 550 °C, respectively.[51] For the $BaZr_{0.7}Pr_{0.1}Y_{0.2}O_{3-\delta}$ (BZPY)-based cell, the conductivity of the BZPY film was about 1.5×10^{-3} S.cm^{-1} at 600 °C.[21] The

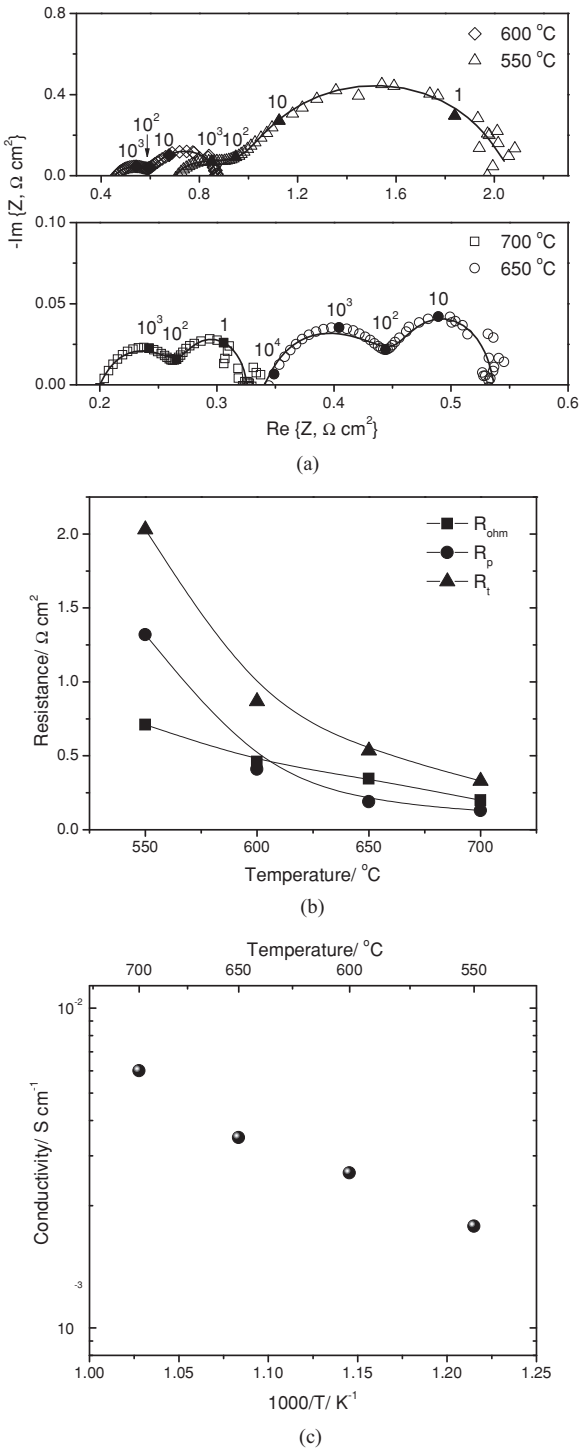

Figure 9. (a) Electrochemical impedance spectra of the cell measured under open circuit conditions. The lines are the fitting results, and the numbers are the frequencies in hertz. (b) The estimated ohmic resistance (R_{ohm}), polarization resistances (R_p), and total resistance (R_t) of the cell. (**c**) Arrhenius plots of the electrical conductivity of BZSY film under fuel cell conditions.

high conductivity of the BZSY film reveals that drop coating is an effective low-cost technique to fabricate high-quality electrolyte films. As is reported, the total conductivity of $BaZrO_3$-based films is significantly restricted by the poor conductivity of grain boundaries. Bi et al.[54] developed a novel method of preparing sinteractive anodic powders to get dense and highly conductive BZY films with larger grain size. D. Pergolesi et al.[59] successfully fabricated a grain-boundary-free BZY film by PLD, and the film showed the largest proton conductivity ever reported for BZY samples, being 0.11 S cm^{-1} at 500 °C. Therefore, there is great potential to improve the proton conductivity of BZSY films by improving the preparation process or employing new techniques to fabricate films with less grain boundaries. One more point, compared to the R_p values of some $BaZrO_3$-based cells (Table 1), the R_p values of the cell studied in this work are still a bit larger. R_p is mainly determined by the electrode materials and related microstructures. Therefore, research attention should also be focused on developing novel active cathode materials, engineering electrode microstructures and optimizing electrode/electrolyte interfaces, to further decrease the polarization of BZSY-based fuel cells.

3. Conclusion

In summary, $BaZr_{0.7}Sn_{0.1}Y_{0.2}O_{3-\delta}$ (BZSY), which evolves from $BaZr_{0.8}Y_{0.2}O_{3-\delta}$(BZY) by partial substituting Zr^{4+} with Sn^{4+}, was developed as a new chemically stable proton-conducting electrolyte material for low-temperature SOFCs. BZSY exhibits significantly enhanced hydration ability and higher electrical conductivity than BZY. Fully dense and highly conductive BZSY electrolyte film was successfully fabricated on NiO–BZSY substrate. Peak power densities of the single cell with a 12-μm-thick BZSY electrolyte film achieved 360, 292, 214, and 146 mW cm^{-2} at 700, 650, 600, and 550 °C, respectively, which is the best performance for $BaZrO_3$-based SOFCs to date. The present result is a significant progress for proton-conducting SOFCs. It is demonstrated that desirable electrochemical performance can be obtained using $BaZrO_3$-based electrolytes and BZSY is indeed a promising chemically stable electrolyte material for high performance proton-conducting SOFCs.

4. Experimental Section

BZSY and BZY powders used for preparing pellets for conductivity measurement were synthesized via a modified combustion process.[51] $Ba(CH_3COO)_2$, $Zr(NO_3)_4{\cdot}5H_2O$, SnO_2, and Y_2O_3 served as the raw materials. After the combustion, the as-prepared powders were calcined at 1100 °C for 6 h in air to obtain BZSY or BZY powders with a cubic perovskite structure. BZSY and BZY pellets were prepared by uniaxially pressing the corresponding powders and eventually sintered at 1650 °C for 10 h. The relative density of the sintered pellet was estimated via the Archimedes method, achieving 83% and 80% for BZSY and BZY, respectively. BZY and BZSY powders used for thermogravimetric analysis (TGA) and X-ray photoelectron spectroscopy (XPS) analysis were prepared by the solid-state reaction. For BZSY, appropriate amounts of $BaCO_3$, ZrO_2, SnO_2, and Y_2O_3 were mixed thoroughly by ball-milling for 24 h, and ethanol was added during the milling. After dried in the oven, the mixed powders were ground manually by an agate mortar and pestle and then fired at 1100 °C for 5 h in air. Subsequently, the powders were ground thoroughly again and ultimately fired at 1400 °C for 5 h in air to obtain BZSY powders with a perovskite structure.

Phase composition of the BZSY and BZY powders were identified by an X-ray diffractometer (Rigaku TTR-III) using CuKα radiation. BZSY and BZY were hydrated by annealing the powders at 200 °C for 24 h in flowing wet air (3% H_2O). TGA was carried out for the samples from 50–800 °C using a DTG-60H (Shimadzu) instrument with a heating rate of 5 °C min^{-1} in flowing air. The XPS spectra of the powders were collected using an X-ray photoelectron spectrometer (ESCALAB250, Thermo-VG Scientific, UK) using monochromatized Al Kα radiation (1486.92 eV). Measurements were performed in a Constant Analyzer Energy (CAE) mode with 70 eV pass energy for survey spectra and 20 eV for high resolution spectra. Microstructures of the BZSY pellet, BZSY film, and single cell were observed by scanning electron microscopy (SEM, LEO 1530).

The total electrical conductivity of the sintered pellets was studied via a two-point method using an impedance analyzer (CHI604B, Chenhua Inc., Shanghai) with an amplitude of 5 mV in the frequency range from 100 kHz to 0.1 Hz. Pt paste was painted on both sides of the sintered pellets as electrodes and then annealed at 950 °C for 1 h to remove the residual organics. Dry gas was nominally dry. Wet gas was achieved after flowing through a bubbler at room temperature. The gas flow rates were all set to 60 mL min^{-1}. During the measurement, the sample was held for 0.5 h at each temperature under all atmospheres before measuring. Besides, the conductivity measurement was performed in the following sequence: dry H_2, wet $H_2(H_2O)$, wet He (H_2O), dry He, and wet He (D_2O).

The BZSY electrolyte film was prepared by a drop-coating process[60] on the NiO–BZSY (weight ratio 65:35) anode substrate followed by co-firing at 1400 °C for 5 h in static air to get a half cell with a fully dense electrolyte film. For full cell preparation, $Sm_{0.5}Sr_{0.5}CoO_{3-\delta}$–$Ce_{0.8}Sm_{0.2}O_{2-\delta}$ (SSC–SDC, weight ratio 3:2) composite cathode slurry was brush-painted onto the BZSY electrolyte film, followed by firing at 950 °C for 2 h in air to form a porous cathode layer with an effective cathode area of 0.3 cm^2. Silver wire and silver paste was used for current collection. For fuel cell performance measurement, the single cell was sealed onto an alumina fuel cell testing fixture with ceramic paste (Ceramabond 552, Aremco). Wet hydrogen (3% H_2O) and static air was used as the fuel and the oxidant, respectively. The single cell was tested using an Arbin multi-channel electrochemical testing system (MSTAT). The flow rate of the fuel gas was about 30 mL min^{-1}. Electrochemical impedance spectra of the cell were performed using a Solartron 1255 HF frequency response analyzer, interfaced with an EG&G PAR potentiostat model 273A with an amplitude of 10 mV in the frequency range from 100 kHz to 0.1 Hz.

Acknowledgements

This work was supported by the Natural Science Foundation of China (Grant No. 21076204) and the Ministry of Science and Technology of China (Grant No. 2012CB215403).

Received: December 16, 2012
Revised: March 1, 2013
Published online: May 8, 2013

[1] B. C. Steele, A. Heinzel, *Nature* **2001**, *414*, 345.
[2] N. P. Brandon, S. Skinner, B. C. H. Steele, *Annu. Rev. Mater. Res.* **2003**, *33*, 183.
[3] E. D. Wachsman, K. T. Lee, *Science* **2011**, *334*, 935.
[4] T. Suzuki, Z. Hasan, Y. Funahashi, T. Yamaguchi, Y. Fujishiro, M. Awano, *Science* **2009**, *325*, 852.
[5] F. Han, R. Muecke, T. Van Gestel, A. Leonide, N. H. Menzler, H. P. Buchkremer, D. Stover, *J. Power Sources* **2012**, *218*, 157.
[6] H. Huang, M. Nakamura, P. C. Su, R. Fasching, Y. Saito, F. B. Prinz, *J. Electrochem. Soc.* **2007**, *154*, B20.
[7] J. B. Goodenough, *Annu. Rev. Mater. Res.* **2003**, *33*, 91.
[8] K. Eguchi, T. Setoguchi, T. Inoue, H. Arai, *Solid State Ionics* **1992**, *52*, 165.
[9] Q. L. Liu, K. A. Khor, S. H. Chan, X. J. Chen, *J. Power Sources* **2006**, *162*, 1036.
[10] D. F. Yang, X. G. Zhang, S. Nikumb, C. Deces-Petit, R. Hui, R. Maric, D. Ghosh, *J. Power Sources* **2007**, *164*, 182.
[11] Z. G. Lu, J. Hardy, J. Templeton, J. Stevenson, D. Fisher, N. J. Wu, A. Ignatiev, *J. Power Sources* **2012**, *210*, 292.
[12] J. S. Ahn, D. Pergolesi, M. A. Camaratta, H. Yoon, B. W. Lee, K. T. Lee, D. W. Jung, E. Traversa, E. D. Wachsman, *Electrochem. Commun.* **2009**, *11*, 1504.
[13] W. P. Sun, W. Liu, *J. Power Sources* **2012**, *217*, 114.
[14] C. Zuo, S. Zha, M. Liu, M. Hatano, M. Uchiyama, *Adv. Mater.* **2006**, *18*, 3318.
[15] L. Yang, S. Wang, K. Blinn, M. Liu, Z. Liu, Z. Cheng, M. Liu, *Science* **2009**, *326*, 126.
[16] Y. Yamazaki, R. Hernandez-Sanchez, S. M. Haile, *Chem. Mater.* **2009**, *21*, 2755.
[17] F. L. Chen, O. T. Sorensen, G. Y. Meng, D. K. Peng, *J. Mater. Chem.* **1997**, *7*, 481.
[18] C. S. Tu, R. R. Chien, V. H. Schmidt, S. C. Lee, C. C. Huang, C. L. Tsai, *J. Appl. Phys.* **2009**, *105*, 103504.
[19] P. Babilo, S. M. Haile, *J. Am. Ceram. Soc.* **2005**, *88*, 2362.
[20] S. W. Tao, J. T. S. Irvine, *Adv. Mater.* **2006**, *18*, 1581.
[21] E. Fabbri, L. Bi, H. Tanaka, D. Pergolesi, E. Traversa, *Adv. Funct. Mater.* **2011**, *21*, 158.
[22] W. P. Sun, Z. W. Zhu, Z. Shi, W. Liu, *J. Power. Sources.* **2013**, *229*, 95.
[23] D. Pergolesi, E. Fabbri, E. Traversa, *Electrochem. Commun.* **2010**, *12*, 977.
[24] J. H. Shim, J. S. Park, J. An, T. M. Guür, S. Kang, F. B. Prinz, *Chem. Mater.* **2009**, *21*, 3290.
[25] M. A. Azimova, S. McIntosh, *J. Electrochem. Soc.* **2010**, *157*, B1397.
[26] Y. Guo, Y. Lin, R. Ran, Z. Shao, *J. Power Sources* **2009**, *193*, 400.
[27] R. D. Shannon, *Acta Crystallogr. A* **1976**, *32*, 751.
[28] W. Chen, H. Y. Gao, Y. Yang, P. B. Lin, J. Yuan, W. F. Shangguan, J. C. Su, Y. Z. Sun, *Acta Phys.-Chim. Sin.* **2012**, *28*, 2911.
[29] V. Dimitrov, T. Komatsu, R. Sato, *J. Ceram. Soc. Jpn.* **1999**, *107*, 21.
[30] T. Honma, R. Sato, Y. Benino, T. Komatsu, V. Dimitrov, *J. Non.-Cryst. Solids* **2000**, *272*, 1.
[31] V. Dimitrov, T. Komatsu, *Phys. Chem. Glasses* **2003**, *44*, 357.
[32] Q. Zeng, Y. B. Zu, C. G. Fan, C. S. Chen, *J. Membrane Sci.* **2009**, *335*, 140.
[33] K. D. Kreuer, *Solid State Ionics* **1997**, *97*, 1.
[34] K. D. Kreuer, *Solid State Ionics* **1999**, *125*, 285.
[35] S. Takeda, M. Fukawa, Y. Hayashi, K. Matsumoto, *Thin Solid Films* **1999**, *339*, 220.
[36] K. R. Wu, J. J. Wang, W. C. Liu, Z. S. Chen, J. K. Wu, *Appl. Surf. Sci.* **2006**, *252*, 5829.
[37] P. A. Grutsch, M. V. Zeller, T. P. Fehlner, *Inorg. Chem.* **1973**, *12*, 1431.
[38] P. Singh, B. J. Brandenburg, C. P. Sebastian, P. Singh, S. Singh, D. Kumar, O. Parkash, *Jpn. J. Appl. Phys.* **2008**, *47*, 3540.
[39] K. D. Kreuer, *Annu. Rev. Mater. Res.* **2003**, *33*, 333.
[40] P. Babilo, T. Uda, S. M. Haile, *J. Mater. Res.* **2007**, *22*, 1322.
[41] Y. Yamazaki, R. Hernandez-Sanchez, S. M. Haile, *J. Mater. Chem.* **2010**, *20*, 8158.
[42] A. S. Nowick, A. V. Vaysleyb, *Solid State Ionics* **1997**, *97*, 17.
[43] L. Bi, E. Fabbri, Z. Sun, E. Traversa, *Energy Environ. Sci.* **2011**, *4*, 409.
[44] Z. T. Tao, L. Bi, Z. W. Zhu, W. Liu, *J. Power Sources* **2009**, *194*, 801.
[45] Z. W. Zhu, Z. T. Tao, L. Bi, W. Liu, *Mater. Res. Bull.* **2010**, *45*, 1771.
[46] B. Lin, H. P. Ding, Y. C. Dong, S. L. Wang, X. Z. Zhang, D. Fang, G. Y. Meng, *J. Power Sources* **2009**, *186*, 58.
[47] Z. T. Tao, L. Bi, L. T. Yan, W. P. Sun, Z. W. Zhu, R. R. Peng, W. Liu, *Electrochem. Commun.* **2009**, *11*, 688.

[48] L. Zhao, B. B. He, Z. Q. Xun, H. Wang, R. R. Peng, G. Y. Meng, X. Q. Liu, *Int. J. Hydrogen Energy* **2010**, *35*, 753.
[49] L. Bi, S. Q. Zhang, S. M. Fang, Z. T. Tao, R. R. Peng, W. Liu, *Electrochem. Commun.* **2008**, *10*, 1598.
[50] F. Zhao, F. L. Chen, *Int. J. Hydrogen Energy* **2010**, *35*, 11194.
[51] W. P. Sun, L. T. Yan, Z. Shi, Z. W. Zhu, W. Liu, *J. Power Sources* **2010**, *195*, 4727.
[52] Z. Sun, E. Fabbri, L. Bi, E. Traversa, *Phys. Chem. Chem. Phys.* **2011**, *13*, 7692.
[53] Z. Sun, E. Fabbri, L. Bi, E. Traversa, *J. Am. Ceram. Soc.* **2012**, *95*, 627.
[54] L. Bi, E. Fabbri, Z. Sun, E. Traversa, *Energy Environ. Sci.* **2011**, *4*, 1352.
[55] E. Fabbri, L. Bi, J. L. M. Rupp, D. Pergolesi, E. Traversa, *RSC Adv.* **2011**, *1*, 1183.
[56] L. Bi, E. Fabbri, Z. Sun, E. Traversa, *Solid State Ionics* **2011**, *196*, 59.
[57] J. Xiao, W. P. Sun, Z. W. Zhu, Z. T. Tao, W. Liu, *Mater. Lett.* **2012**, *73*, 198.
[58] I. Luisetto, S. Licoccia, A. D'Epifanio, A. Sanson, E. Mercadelli, E. Di Bartolomeo, *J. Power Sources* **2012**, *220*, 280.
[59] D. Pergolesi, E. Fabbri, A. D'Epifanio, E. Di Bartolomeo, A. Tebano, S. Sanna, S. Licoccia, G. Balestrino, E. Traversa, *Nat. Mater.* **2010**, *9*, 846.
[60] M. F. Liu, D. H. Dong, R. R. Peng, J. F. Gao, J. Diwu, X. Q. Liu, G. Y. Meng, *J. Power Sources* **2008**, *180*, 215.